Uranium (III) precipitation in molten chloride by wet argon sparging

Jean-François Vigier, Annabelle Laplace, Catherine Renard, Manuel Miguirditchian, Francis Abraham

Uranium (III) precipitation in molten chloride by wet argon sparging

Jean-François Vigier [a, b, *], Annabelle Laplace [a], Catherine Renard [b], Manuel Miguirditchian [a], Francis Abraham [b]

[a] CEA, Nuclear Energy Division, Radiochemistry & Processes Department, F-30207 Bagnols sur Cèze, France
[b] Unité de Catalyse et de Chimie du Solide, UCCS UMR CNRS 8181, Univ. Lille Nord de France, ENSCL-USTL, B.P. 90108, 59652 Villeneuve d'Ascq Cedex, France

HIGHLIGHTS

- Precipitation of Uranium (III) is quantitative in molten salt LiCl-CaCl$_2$ (30—70 mol%).
- The salt is oxoacid with a water dissociation constant of $10^{-4.0}$ at 705 °C.
- Volatility of uranium chloride is strongly reduced in reductive conditions.
- Coprecipitation of U(III) and Nd(III) leads to a consecutive precipitation of the two elements.

GRAPHICAL ABSTRACT
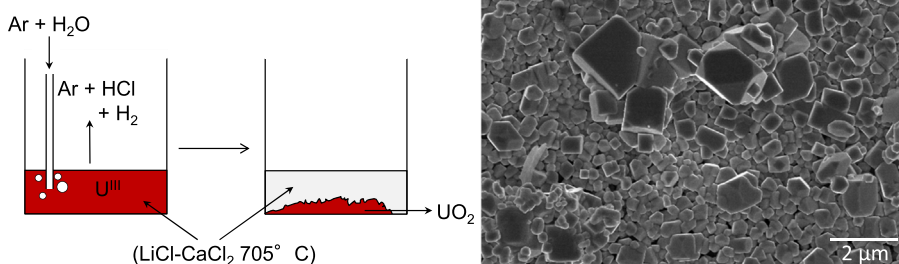
ARTICLE INFO

ABSTRACT

In the context of pyrochemical processes for nuclear fuel treatment, the precipitation of uranium (III) in molten salt LiCl-CaCl$_2$ (30—70 mol%) at 705 °C is studied. First, this molten chloride is characterized with the determination of the water dissociation constant. With a value of $10^{-4.0}$, the salt has oxoacid properties. Then, the uranium (III) precipitation using wet argon sparging is studied. The salt is prepared using UCl$_3$ precursor. At the end of the precipitation, the salt is totally free of solubilized uranium. The main part is converted into UO$_2$ powder but some uranium is lost during the process due to the volatility of uranium chloride. The main impurity of the resulting powder is calcium. The consequences of oxidative and reductive conditions on precipitation are studied. Finally, coprecipitation of uranium (III) and neodymium (III) is studied, showing a higher sensitivity of uranium (III) than neodymium (III) to precipitation.

© 2016 Elsevier B.V. All rights reserved.

1. Introduction

Spent nuclear fuel management represents one of the most important issues related to the sustainable development of nuclear energy. In France, spent nuclear fuel is currently recycled at industrial scale by the hydrometallurgical PUREX process allowing selective recovery of uranium and plutonium for new fuel fabrication. However, with the development of Generation IV reactors, many researches are still focused on new processes, for minor actinides (americium, neptunium and curium) recovery together with uranium and plutonium. For such applications, alternatives to hydrometallurgical processes are also considered, such as pyrochemical processes showing specific advantages: no sensitivity to radiolysis and a reduced criticality risk for example [1,2].

At CEA (French Atomic Energy and Alternative Energies Commission), one of the considered pyrochemical processes is based on

* Corresponding author. Current address: European Commission, Joint Research Centre (JRC), Institute for Transuranium Elements (ITU), Postfach 2340, 76125 Karlsruhe, Germany.
E-mail address: jean-francois.vigier@ec.europa.eu (J.-F. Vigier).

selective liquid–liquid reductive extraction of actinides versus lanthanides in a molten aluminium alloy [3] (Fig. 1). After this separating step, actinides are back-extracted in the LiCl-CaCl$_2$ (30–70 mol%) molten chloride salt at high temperature (705 °C) [4]. Solubilized at the oxidation state (III) in the salt, actinides conversion to AnO$_2$ oxides needs to be considered for the fabrication of new nuclear fuel. The present study is mainly focused on U(III) chloride conversion to UO$_2$ in the molten LiCl-CaCl$_2$.

The chemistry of uranium in molten chloride is well described by Martinot et al. [5] through the Pourbaix diagram in eutectic LiCl-KCl at 450 °C. This diagram presents the stability of soluble and insoluble uranium species as a function of the potential and the O^{2-} concentration in the salt. It highlights the rich diversity of stable oxidation states of uranium in these medias with, for low O^{2-} concentration the presence of many soluble species U^{3+}, U^{4+}, UO$_2^+$, UO$_2^{2+}$ and for higher O^{2-} concentration, the insoluble species UO$_2$, UO$_3$ and U$_3$O$_8$. Metallic uranium is also stable in molten chloride at the lowest potential. Thereby, in order to obtain solid UO$_2$ from solubilized U^{3+}, the precipitation method needs to provide oxide ion O^{2-} and to be moderately oxidizing for an oxidation of uranium from III to IV, but not higher. Moreover, different uranium precipitates are formed by varying the molten chloride nature. If no solid uranium (III) compounds was reported in these medias and uranium (IV) is only presented as UO$_2$ [5–9], higher oxidation states can produce numerous compounds as MUO$_3$, M$_2$UO$_4$, M$_2$U$_2$O$_7$ (M = alkali metal) or M'UO$_4$, M'U$_2$O$_7$ (M' = alkaline earth metal) [5,10]. These compounds emphasize the importance of a moderate oxidative way of precipitation to avoid an oxidation over the oxidation state (IV) and a pollution of the final powder with alkaline or alkaline hearth metal.

In this study, the precipitation of uranium (III) was done by wet argon sparging. This technique has been patented for pyroprocessing of actinides from spent nuclear fuel [11], and a similar technique has been used in the past for crystal growth of UO$_2$ and ThO$_2$ in fluoride molten salt [12]. Wet argon sparging has already shown interesting performances for the precipitation of cerium (III) and neodymium (III) [13,14]. In the first part of the publication, the Oxo-acidity property of the salt LiCl-CaCl$_2$ (30–70 mol%) has been determined using potentiometric method. The precipitation of uranium has been then studied in several conditions (standard, oxidative and reductive). Finally, as a preliminary study of uranium (III) co-precipitation with others actinides (III) (plutonium and/or minor actinides), the co-precipitation of uranium (III) and neodymium (III) by wet argon sparging has been investigated.

2. Experimental

2.1. General features

LiCl-CaCl$_2$ (30–70 mol%) melt was prepared from LiCl (Sigma Aldrich, 99%) and CaCl$_2$ (Alpha Aesar 96%). Uranium chloride was synthesized at the laboratory and anhydrous NdCl$_3$ (Aldrich, 99.9% under argon) was used. The LiCl-CaCl$_2$ salt mixture was introduced

in a vitreous carbon crucible (SGL Carbon, Sigradur type), itself placed into a leak tight quartz reactor heated in a vertical tubular furnace. The salt was first dehydrated by heating under vacuum at 300 °C during 6 h, and then heated to 705 °C (2 °C min^{-1}) under 2 NL h^{-1} of dry argon (Air Liquide, Ar N60, H$_2$O < 0.6 ppm, O$_2$ < 0.1 ppm). The complete fusion of the salt occurred at 680 °C [15]. The bath temperature was measured with an S-type thermocouple (±1 °C) sheathed into a glassy carbon closed end tube (Carbone Lorraine, V25 type) immersed into the molten salt. Uranium trichloride and/or neodymium trichloride was then added to the previously dehydrated molten LiCl-CaCl$_2$.

The experimental device used for precipitation experiments is Fig. 2 and has been previously described [13]. Uranium precipitation was performed by sparging wet argon through a glassy carbon tube (SGL Carbon, Sigradur type) in the molten chloride. Wet argon was obtained by argon sparging (2 NL h^{-1} through a PTFE frit) in water at 20 °C, in a dedicated bottle placed upstream of the reactor. The saturation pressure of water vapor in these temperature conditions is 2352 Pa [16]. The reaction of water in the fused salt produced hydrochloric acid gas neutralized downstream by a ~0.1 M NaOH solution.

After the precipitation, wet argon was replaced by dry argon. After salt sampling for further ICP analyses, the salt was cooled to room temperature under argon atmosphere, recovered from the crucible and dissolved in 100 mL of water. The precipitate was filtered, washed several times with deionized water and dried at room temperature. The final powder was analyzed by XRD, TGA and SEM analysis.

2.2. UCl$_3$ synthesis

Uranium trichloride (UCl$_3$) was selected as starting material for U(III) conversion experiments in molten salt and was synthesized from uranium oxide U$_3$O$_8$ in two steps: conversion to UCl$_4$ and then to UCl$_3$. Uranium chlorides being highly hygroscopic products, they were stored and manipulated in Argon glove box.

UCl$_4$ was synthesized by action of CCl$_4$ vapour in argon flow (5 NL h^{-1}) on 70 g of U$_3$O$_8$ at 500 °C [17]. The experimental device and crucibles previously described were used, replacing the water by CCl$_4$ in the bottle placed upstream of the reactor. This way of chlorination was convenient to produce large amount of material, however some uranium was lost due to the formation of volatile species (U(VI) and U(V) chlorides) which condensed on the cold parts of the reactor. The reaction was done twice (first 24 h and then 4 h) to improve the conversion yield. 52.6 g of well crystalline green powder, characteristic of UCl$_4$ were obtained.

The second step consisted in reducing a slight excess of UCl$_4$ (52.6 g) in contact with metallic zinc (4.29 g) at 500 °C [18] and under argon flow (2 NL h^{-1}) in the quartz reactor, following the equation:

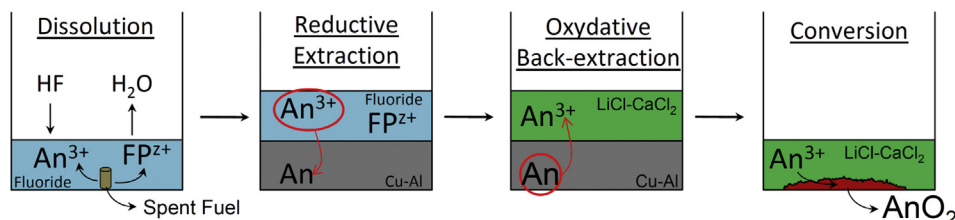$$2UCl_4 + Zn^0 = 2UCl_3 + ZnCl_2 \tag{1}$$

Fig. 1. Schematic description of the main steps considered in the CEA pyrochemical liquid–liquid extraction process. "FP" stands for Fission Product, and "An" for Actinides.
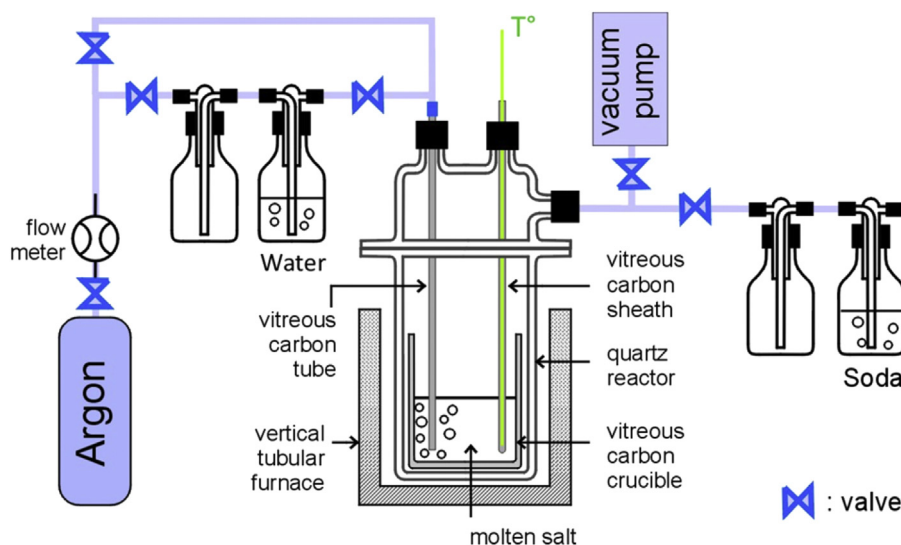
Fig. 2. Experimental set-up for uranium precipitation in molten LiCl-CaCl₂ by humid argon sparging.

The reaction was maintained for 3 h, and then the temperature was slowly increased up to 800 °C (0.5 °C min^{-1}) to release ZnCl$_2$ and the excess of UCl$_4$ by volatilization (Table 1). 39 g of acicular dark powder were obtained after cooling at room temperature. The absence of zinc was checked by ICP-AES analysis, and UCl$_3$ was clearly identified by X-Ray diffraction (Fig. 3). The UCl$_3$ synthesized powder contained less than 7 wt.% of UO$_2$, evaluated by selective dissolution of the powder in water, filtration and weighting of the insoluble UO$_2$. This gave a reaction yield of about 80%. In the following text the term "UCl$_3$" will refer to this powder.

2.3. Uranium precipitation experiments

Different uranium precipitation experiments were conducted. The precipitation conditions slightly differed from one to other (atmosphere, redox conditions, Nd coprecipitation) and are summarized in Table 2. 0.9−1.45 g of UCl$_3$ were added to 20 g of previously dehydrated and molten LiCl-CaCl$_2$ salt. The precipitation experiments were run at 705 °C for 1 h−6 h with wet argon flow at 2 NL h^{-1} (saturated at 20 °C). The first experiment U1 was conducted as previously described with 1.45 g of UCl$_3$ during 6 h. In the second one (U2), the wet argon flow in the molten salt was slightly contaminated with oxygen. The amount of air introduced in the wet argon atmosphere was not well controlled but was estimated to be around 1%. In the third one (U3), a 0.61 g piece of metallic uranium was added to the LiCl-CaCl$_2$-UCl$_3$ solution before wet argon sparging. The objective was to maintain reductive conditions in the molten salt during uranium precipitation. The amount of metallic uranium consumed during the precipitation was determined from the mass difference of the metal before and after the precipitation.

Two uranium-neodymium co-precipitation (U-Nd1 and U-Nd2), with an equimolar proportion of the two elements ($n_U = n_{Nd} = 2.6$ mmol) were run during 1 h and 6 h, respectively.

Table 1
Melting and boiling temperatures of the compounds related to the UCl₃ synthesis.

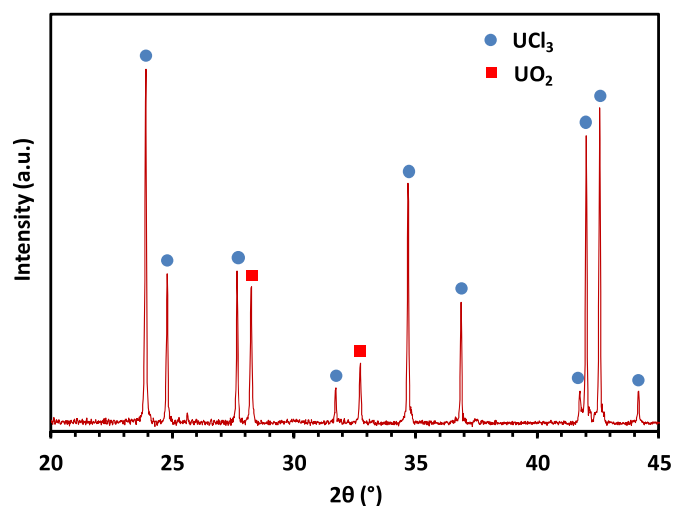| Compound	Melting point (°C)	Boiling point (°C)	Reference
Zn^0	405	907	[16]
UCl$_4$	590	789	[17]
ZnCl$_2$	283	732	[16]
UCl$_3$	835	1657	[17]

Fig. 3. XRD patterns of the "UCl₃" powder used as starting material for the preparation of molten salt containing solubilized uranium (III).

2.4. Electrodes and potentiometric instrumentation

In order to characterize the "oxoacid power" of the LiCl-CaCl$_2$ molten salt, O^{2-} oxide ions concentration in the molten salt was measured by potentiometry.

Potentiometric measurements were performed with a two-electrode set-up connected to a potentiostat-galvanostat Autolab PG Stat 30 controlled with the Autolab software package (Metrohm).

The electrodes used consisted of an AgCl/Ag reference electrode and a selective oxide ions membrane electrode (YSZE electrode). The reference electrode was made of a silver wire (1 mm Ø, Goodfellow, 99.99%) dipped into a closed-end mullite tube (OMG France, 6−4 mm Ø) containing a 0.75 mol kg^{-1} silver chloride (Aldrich, 99%) solution in the LiCl−CaCl$_2$. The oxide ions membrane electrode was constituted by a closed-end tube of ZrO$_2$ stabilized with 8 wt.% Y$_2$O$_3$ (Sceram, 6−4 mm Ø), containing a constant O^{2-} ion concentration (0.1 mol kg^{-1} in LiCl−CaCl$_2$, introduced as solid Li$_2$CO$_3$ (Aldrich, 99%)) and an internal AgCl/Ag reference (0.75 mol kg^{-1} AgCl with a 1 mm Ø silver wire (Goodfellow,

Table 2
Uranium precipitation conditions.

Experiment	U1	U2	U3	U-Nd1	U-Nd2
Temperature (°C)	705	705	705	705	705
Wet argon flow (NL h^{-1}) (saturated at 20°C)	2	2	2	2	2
Atmosphere	Ar/H$_2$O	Ar/H$_2$O with few O$_2$ (~1%)	Ar/H$_2$O	Ar/H$_2$O	Ar/H$_2$O
Duration (h)	6	6	6	6	1
n_{H_2O} introduced (mmol)	11.3	11.3	11.3	11.3	1.9
LiCl-CaCl$_2$ (g)	20	20	20	20	20
UCl$_3$ (g)	1.45	1.45	1.45	0.9	0.9
Metallic U (g)	0	0	0.61	0	0
NdCl$_3$ (g)	0	0	0	0.65	0.65

99.99%)).

O^{2-} concentration was determined by measuring the e. m.f. between the reference and the YSZE electrode and using a calibration curve obtained by adding controlled quantities of Li$_2$CO$_3$ (Aldrich, 99%) in the salt under Ar atmosphere [19].

2.5. Determination of the oxoacidity constant of the HCl/H$_2$O system

For this experiment, specific anhydrous reactants were used. 30 g of LiCl-CaCl$_2$ (30–70 mol%) were prepared from LiCl (Sigma Aldrich, 99.998%, sealed under Ar) and CaCl$_2$ (Sigma Aldrich, 99.99%, sealed under Ar) and were heated to 705 °C (2 °C min^{-1}) under argon atmosphere. Reference and YSZE electrodes were introduced in the molten salt. Argon with different P^2_{HCl}/P_{H_2O} ratios was bubbled in the molten salt and the YZSE electrode stabilized potential was measured versus the reference electrode for each ratio, as described by Castrillejo et al. [20].

The experimental device and crucibles previously described were used, replacing the water by HCl solution in the bottle placed upstream of the reactor. The different HCl and H$_2$O partial pressure ratios were obtained by bubbling argon (2 NL h^{-1}) through thermostated HCl solution at 25 °C with different successive concentrations (35.6%, 33.6%, 31.6%, 29.7% and 27.7%). The partial pressures of HCl and H$_2$O in the argon flow were deduced using thermodynamic table [21]. In order to get a better stabilization of the pressure ratio, two HCl bottles were serially connected. The two bottles were initially filled with 200 g of 37% HCl solution (Rectapur). For each pressure ratio, specific quantities of water were introduced thanks to a dedicated opening, to obtain the respective HCl solution concentration. After the YSZE electrode potential stabilization, a sample was taken from the second HCl solution and HCl concentration was determined with a standard 1 M NaOH solution titration. Then, controlled quantity of water was introduced in the two HCl solutions to obtain the next conditions.

2.6. Analytical techniques

2.6.1. Induced coupled plasma analysis-atomic emission spectroscopy (ICP-AES)

The precipitation yields were calculated from the concentration of soluble uranium and neodymium remaining in the molten salt at the end of the precipitation. The concentrations of soluble species in the salt were measured by Induced Coupled Plasma Atomic Emission Spectroscopy (ICP-AES). About 100 mg of samples, extracted from the hot mixture by suction through a quartz tube at the end of the precipitation, were dissolved in 100 mL of water and filtered to remove any precipitate. The acidification of the solution with nitric acid stabilized the solubilized elements. The analyses of the solutions gave the amount of unreacted uranium in the molten salt. To avoid any matrix effect on the ICP-AES measurements, the

standard range was made with the same concentration of LiCl, CaCl$_2$ and HNO$_3$.

2.6.2. X-ray diffraction (XRD)

The precipitates powder X-ray diffraction patterns were recorded using a D8 Advance Bruker diffractometer with Cu Kα radiation and an energy dispersive detector (sol-X), over a 2θ range of 10–80° at 0.02° increments. The profile fitting and the cell parameters refinements were performed using the powder option of JANA2006 [22].

2.6.3. Scanning electron microscope (SEM)

The morphology of the precipitate was observed with a Scanning Electron Microscope (SEM) Hitachi S4700 with Field Emission Gun (FEG), a cathodoluminescence and an Electron Beam Induced Current (EBIC) system.

2.6.4. Thermogravimetric analysis (TGA)

Thermal analyses were performed under air atmosphere on a Setsys Evolution Thermogravimetric Analyzer from Setaram, in a temperature range from 100 to 800 °C (5 °C min^{-1} heating speed).

2.6.5. Conductimetric analysis

The hydrochloric acid released from the water reaction in molten chloride can be followed by conductimetric evolution of the NaOH solution placed downstream of the reactor. The technique has been previously described [13]. The NaOH solution conductivity was continuously measured during the precipitation reaction. Using this method, the hydrochloric acid flow rate D_{HCl} released from the molten salt can be compared to the water flow rate D_{H_2O} introduced in the media. For example, the relation $D_{HCl} = 2D_{H_2O}$ was obtained for the reaction described by Equation (2).

3. Results and discussion

3.1. Determination of the oxoacidity constant of the HCl/H$_2$O system

Processes, like oxides solubilization or precipitation can be estimated a priori by determining the oxoacidity properties of the molten salt mixtures. The more the oxoacidity properties are important, the more oxides can be solubilized in the salt. For precipitation, molten salt with oxobasic properties are often selected, such as NaCl-KCl and NaCl-CsCl [23]. The oxoacidity properties are generally characterized by the equilibrium constant K_{H_2O} of the reaction 2 in the considered molten salt [19,24]:

$$H_2O_{(g)} + 2Cl^-_{(salt)} = O^{2-}_{(salt)} + 2HCl_{(g)} \tag{2}$$

$$K_{H_2O} = \frac{P^2_{HCl} \cdot [O^{2-}]}{P_{H_2O} \cdot [Cl^-]} \tag{3}$$

With K_{H_2O} (atm.mol.kg^{-1}), P the pressure (atm), [O^{2-}] the oxide concentration (mol.kg^{-1}) and the chloride ions activity being taken as unity. The pO^{2-} value (pO^{2-} = $-$log(a(O^{2-}))) is determined with the potential between the reference and the selective oxide ions membrane electrode (YSZE), following the Nernst's expression:

$$E = E^0 + \frac{2.3RT}{2F}pO^{2-} \tag{4}$$

According to Equation (3), and using the logarithmic form, pO^{2-} is given by:

$$pO^{2-} = pK_{H_2O} + log\left(\frac{P^2_{HCl}}{P_{H_2O}}\right) \tag{5}$$

The experimental pO^{2-} measurement for different HCl and H$_2$O imposed partial pressures in the molten salt leads to the determination of the oxoacidity constant K_{H2O}.

To our knowledge, the oxoacidity constant in the LiCl-CaCl$_2$ molten salt has not been determined yet and this characteristic data is useful for precipitation study. Fig. 4a shows the calibration curve of the YSZE at low pO^{2-} and its verified Nernstian behavior. The experimental measurement of pO^{2-} as a function of the partial pressure ratios log(P$^2_{HCl}$/P$_{H2O}$) leads to a linear variation (Fig. 4b). A pK$_{H2O}$ value of 4.0 ($\pm$0.5) for LiCl-CaCl$_2$ (30–70 mol%) at 705 °C is determined from this variation. Compared to other molten salts and particularly the well-used LiCl-KCl salt (Table 3), the LiCl-CaCl$_2$ salt used in this study shows higher oxoacidity properties, probably due to the presence of the hard divalent cation Ca^{2+} in its composition. Such a salt is *a priori* not favorable to precipitation due to its capability to dissolve oxide ions. The choice of this LiCl-CaCl$_2$ "oxoacidic" salt was motivated by the optimization of the upstream step in the pyrochemical process (ie. actinides back extraction from a metallic aluminium alloy) [25]. However, the more important the oxoacidity properties are, the more the water reaction in the salt is displaced to the right (Equation (2)). This is in favor to the wet argon sparging precipitation and could compensate the first effect.

3.2. Uranium precipitation by wet argon sparging

The uranium (III) precipitation experiment U1 in molten LiCl-CaCl$_2$ (30–70 mol%) by wet argon sparging leads to a brown–red powder (Fig. 5). Unreacted uranium in the salt is not detected with ICP-AES analyses of the sample taken after the end of precipitation. On this basis, the U(III) conversion rate is over 99.9%, deduced from the limit detection of the ICP-AES apparatus. Despite the high oxoacidity of the molten salt used in this study, U(III) conversion in molten salt with wet argon sparging is quantitative. However, during the experiment, a part of uranium is volatilized from the molten salt and condenses on the cold parts of the quartz reactor. This can be explained by the formation of UCl$_4$ during the precipitation. Uranium tetrachloride is volatile at the working temperature (T$_{vap}$ = 789 °C [17]). Due to the use of acidic salt, this volatility is not prevented by complexation [27,28]. The amount of uranium lost by volatilisation is deduced from the weight of the final precipitate. It is estimated at 26% of the initial uranium introduced in the molten salt. This lost is not conflicting with the quantitative conversion rate determined by ICP analysis, but has to be considered as a secondary phenomenon. This volatility is a potential issue for the process.

The precipitate is clearly identified as crystalline UO$_2$ single phase by XRD analysis. The cell parameter of 5.471(1)Å is in good agreement with the published value [29]. This lattice parameter indicates that the uranium oxide has a stoichiometric composition UO$_{2.00}$. The TGA analysis shows a weigh increase of 3.75% during
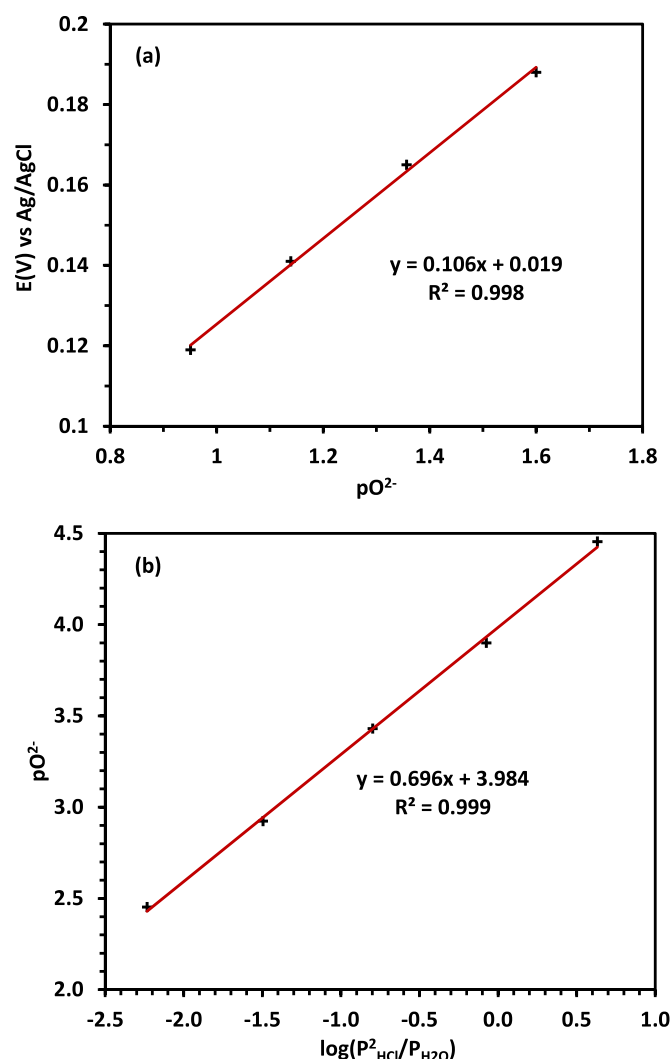

Fig. 4. (a) Calibration of the specific oxide ions electrode (YSZE) in LiCl-CaCl$_2$ (30–70 mol%) at 705 °C. (b) Variation of the pO^{2-} of the molten LiCl-CaCl$_2$ (30–70 mol %) at 705 °C under different HCl and H$_2$O partial pressures.

the oxidation of the precipitate under air atmosphere (Fig. 6) which confirms the uranium dioxide formation (theoretical increase from UO$_2$ to U$_3$O$_8$, 3.95%). The morphology of UO$_2$ shows truncated cubic crystals, with grain size from 0.2 to 2 μm (Fig. 7). The precipitation reaction can thus be written:

$$UCl_{3(salt)} + 2H_2O_{(g)} = UO_{2(solid)} + 3HCl_{(g)} + \frac{1}{2}H_{2(g)} \tag{6}$$
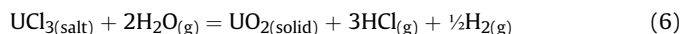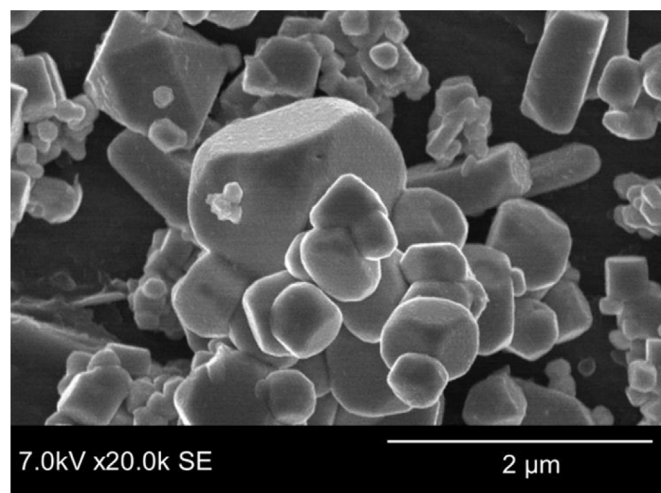
The hydrochloric acid production is monitored by the conductivity measurement of the soda solution downstream the reactor. The theoretical evolution of the NaOH solution conductivity is calculated for two stoichiometries (Table 4). The first one uses the relation D$_{HCl}$ = 2D$_{H2O}$ (Equation (2)) as previously observed for the total reaction of water during lanthanide precipitation [13]. The second one is also based on a total reaction of the introduced water, but takes into account the oxidation property of water during uranium precipitation (Equation (6)), decreasing the HCl release due to the hydrogen formation and leading to the relation D$_{HCl}$ = 1.5D$_{H2O}$. The experimental and calculated evolutions of the conductivity are presented in the Fig. 8. The experimental curve shift is due to the gas volume of reactor and safety bottle between the molten salt and the soda solution which delays the hydrochloric

Table 3
Comparison between K_{H2O} of the molten LiCl-CaCl$_2$ (30—70 mol%) at 705 °C and other molten salts.

Molten chloride	Molar fraction (%)	pK$_{H2O}$ (K$_{H2O}$ in atm.mol.kg^{-1})	Temperature (°C)	Reference
NaCl-KCl	50—50	14	727	[26]
LiCl-KCl	45—55	6.5	727	[26]
CaCl$_2$—NaCl—KCl	10—45—45	5.2	727	[26]
LiCl-CaCl$_2$	30—70	4.0	705	This study
MgCl$_2$-KCl	50—50	2.4	727	[26]
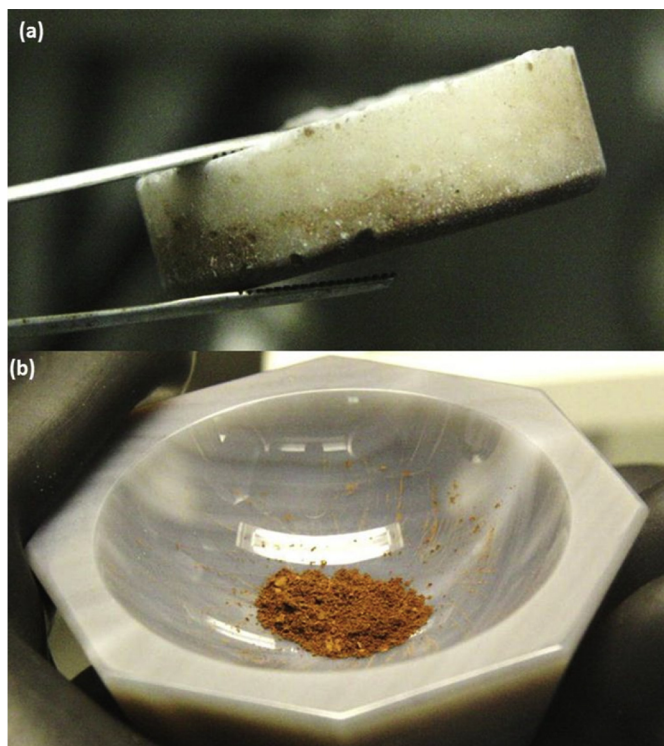
Fig. 5. U1 experiment (a) Picture of LiCl-CaCl$_2$ (30—70 mol%) salt after the end of precipitation and cooling at room temperature containing the uranium precipitate at the bottom. (b) Picture of uranium precipitate after dissolution of the salt in water, filtration and drying.
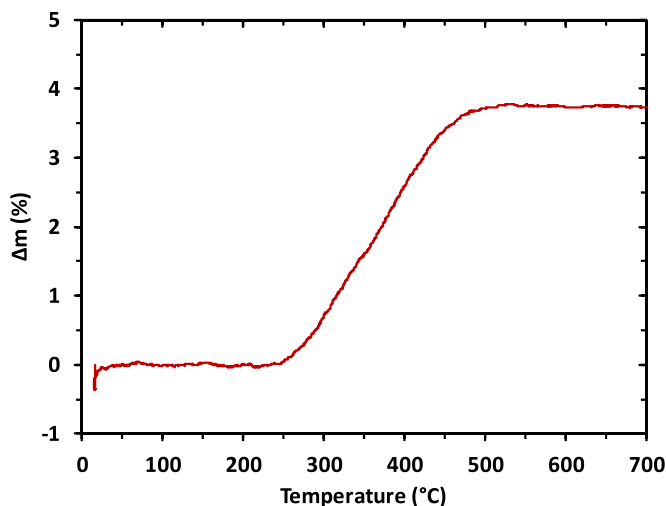

Fig. 6. TGA analysis of uranium precipitate obtained by precipitation of 5 wt% U(III) in LiCl-CaCl2 (30—70 mol%) at 705 °C using wet argon sparging (U1 experiment).

Fig. 7. SEM picture of uranium precipitate showing the morphology of UO$_2$ crystals.

flow in the soda bottle. Considering this equation was already proved by XRD analysis of precipitate, this conductivity variation highlights the total reaction of the introduced water in the molten salt for uranium precipitation. The experimental results are closed to the second model evolution, in agreement with the precipitation reaction 6. Water plays two roles during the uranium (III) precipitation: it oxidizes the actinide (III) to oxidation state (IV) with a release of hydrogen, and it provides oxide ions for the conversion of soluble uranium chloride to insoluble uranium oxide. In contrast to cerium (III) precipitation by wet argon studied previously and giving a mixture of Ce^{III}OCl and Ce^{IV}O$_2$ [13], all the uranium (III) is oxidized into uranium (IV). A part of U(IV) is volatilized as UCl$_4$ and the main part is precipitated, giving uranium dioxide suitable for the fabrication of new nuclear fuel.

The possible calcium and lithium contamination of the precipitate (coming from the solvent) has been checked. A part of the uranium oxide was dissolved in nitric acid and analysed by ICP-AES. The precipitate contains 1.2 wt% of calcium. The lithium concentration is under the apparatus limit detection which corresponds to less than 0.01 wt% of the precipitate.

In the second experiment, the accidental introduction of oxygen during the precipitation has allowed to study the precipitation in more oxidative conditions. The presence of oxygen contamination has significant consequence on the final uranium precipitate (Table 5). The precipitate loses its characteristic brown—red colour and is a black powder (Fig. 9). The XRD pattern shows a biphasic composition (Fig. 10). The UO$_2$ peaks, with the same lattice parameter 5.471(1)Å as observed for U1 experiment, have shoulders at high angles. These peaks show the presence of a second fluorite compound with a smaller cell parameter, 5.435(2) Å. The calcium contamination, controlled after dissolution with ICP-AES analysis, is around 10 wt%. Due to the strong increase of calcium contamination compared to experiment U1, the second fluorite

Table 4
Experimental and calculated data for precipitation and the maximal conductivity evolution of the soda solution downstream the reactor.

Experimental data		Calculated data	
Ar flow rate	2 L h^{-1}	H$_2$O partial vapor pressure [16]	2352 Pa
H$_2$O temperature	20 °C	H$_2$O molar flow rate	0.00189 mol h^{-1}
NaOH solution volume	500 mL	Maximal HCl molar flow rate[a] for $D_{HCl} = 2D_{H2O}$	0.00377 mol h^{-1}
		Maximal HCl molar flow rate[b] for $D_{HCl} = 1.5D_{H2O}$	0.00283 mol h^{-1}
NaOH solution concentration	0.06 mol L^{-1}	Highest conductivity evolution[a] for $D_{HCl} = 2D_{H2O}$	−0.92 mS cm^{-1} h^{-1}
		Highest conductivity evolution[b] for $D_{HCl} = 1.5D_{H2O}$	−0.69 mS cm^{-1} h^{-1}

[a] Considering the reaction: $H_2O_{(g)} + 2Cl^-_{(salt)} = O^{2-}_{(salt)} + 2HCl_{(g)}$.
[b] Considering the reaction: $2H_2O_{(g)} + 3Cl^-_{(salt)} + e^- = 2O^{2-}_{(salt)} + 3HCl_{(g)} + ½H_{2(g)}$.
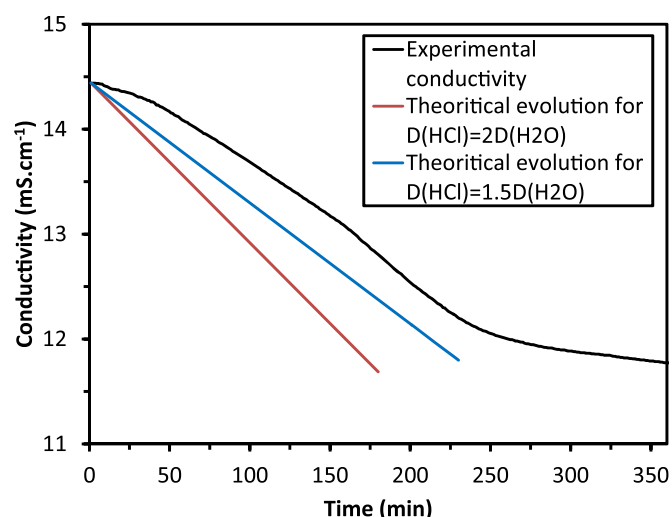
Fig. 8. Experimental and theoretical evolution of the NaOH solution downstream the reactor, in function of the wet argon sparging time for 5 wt% U(III) in LiCl-CaCl2 (30−70 mol%) at 705 °C.

($m_{UCl3} = 1.45$ g, $n_U = 4.2$ mmol). The ratio gives the global equation:

$$U + 2UCl_3 + 6H_2O_{(g)} = 3UO_2 + 6HCl_{(g)} + 3H_{2(g)} \quad (7)$$

The calcium contamination of the precipitate is slightly lower, 0.8 wt.%, than the contamination with the conditions in U1 experiment but is in the same order of magnitude. In these reductive conditions, there is a strong decrease of the uranium lost by volatilisation (6% of initial uranium) which seems to confirm that this phenomenon is caused by volatile UCl$_4$ formation during precipitation, and is mostly avoided with the presence of metallic uranium.

3.3. U(III) and Nd(III) co-precipitation

The precipitation of uranium and neodymium in LiCl-CaCl$_2$ molten salt has been studied through two experiments differentiated by the wet argon sparging time: 6 h for U-Nd1 and 1 h for U-Nd2 (Table 2). The XRD patterns of the precipitates are shown in Fig. 11. For U-Nd1, the precipitate is a mixture of NdOCl and UO$_2$. Uranium and neodymium seem to react independently during the

Table 5
Experimental data for U(III) precipitation experiments at 5 wt% in LiCl-CaCl$_2$ (30−70 mol%) at 705 °C using wet argon sparging.

Experiment	U1	U2	U3
Specific conditions	−	O$_2$ impurities in wet argon	Excess of U^0 in the salt
Colour of precipitate	Brown−Red	Black	Brown−Red
Calcium content in the precipitate (wt%)	1.2	10	0.8
Uranium lost by volatilization (%)	26	28	6
Lattice parameter of UO$_2$ (Å)	5.471 (1)	5.471 (1)	5.470 (1)
Lattice parameter of the second fluorite phase (Å)	−	5.435 (2)	−

phase detected in the powder can be attributed to Ca$_y$U$_{1-y}$O$_{2+x}$ solid solution [30,31]. This second phase could be also attributed to UO$_{2+x}$, with a composition close to the U$_4$O$_9$ oxide ($a/4 = 5.441(1)$Å [27]), due to a partial oxidation of uranium over the oxidation state (IV) induced by the presence of oxygen.

These experiments are a good illustration of the importance of working under moderate oxidative conditions and show the negative consequences of oxygen in wet argon on uranium precipitate in a nuclear fuel fabrication context.

The U3 experiment was undertaken to study the precipitation in more reductive conditions. The uranium (III) precipitation by wet argon sparging is done in presence of metallic uranium in the molten salt. These reductive conditions have no significant consequence on the nature of the uranium precipitate, leading to a brown−red powder, identified by XRD as a single phase UO$_2$ with a cell parameter $a = 5.470(1)$ Å cell parameter (Fig. 10). During the precipitation, 0.51 g of metallic uranium is consumed (2.1 mmol), which is significant compared to the amount of UCl$_3$ used

co-precipitation. The UO$_2$ lattice parameter is 5.470(1)Å, similar than for U precipitation without neodymium. Therefore, there is not significant introduction of neodymium in this oxide [32]. In the same way, the introduction of uranium is not significant in neodymium oxychloride which crystallizes with lattice parameters ($a = 4.025(1)$ Å, 6.775(1) Å) close to the NdOCl reported in literature ($a = 4.025(1)$ Å, 6.784(1) Å [33]). A previous study showed that the precipitation of Nd(III) alone in the same conditions leads to NdOCl oxychloride formation [13]. The U-Nd2 experiment results show that after 1 h of wet argon bubbling, the precipitate contains uranium dioxide, UO$_2$, with lattice parameter $a = 5.471(1)$Å, and only very few NdOCl traces. These results demonstrate that uranium (III) is more sensitive to the precipitation than neodymium (III) and precipitates first while the neodymium ions are still solubilized in the molten chloride. The consecutive reaction of the two elements explains their separation in two compounds in the precipitate and the non-formation of a solid solution.
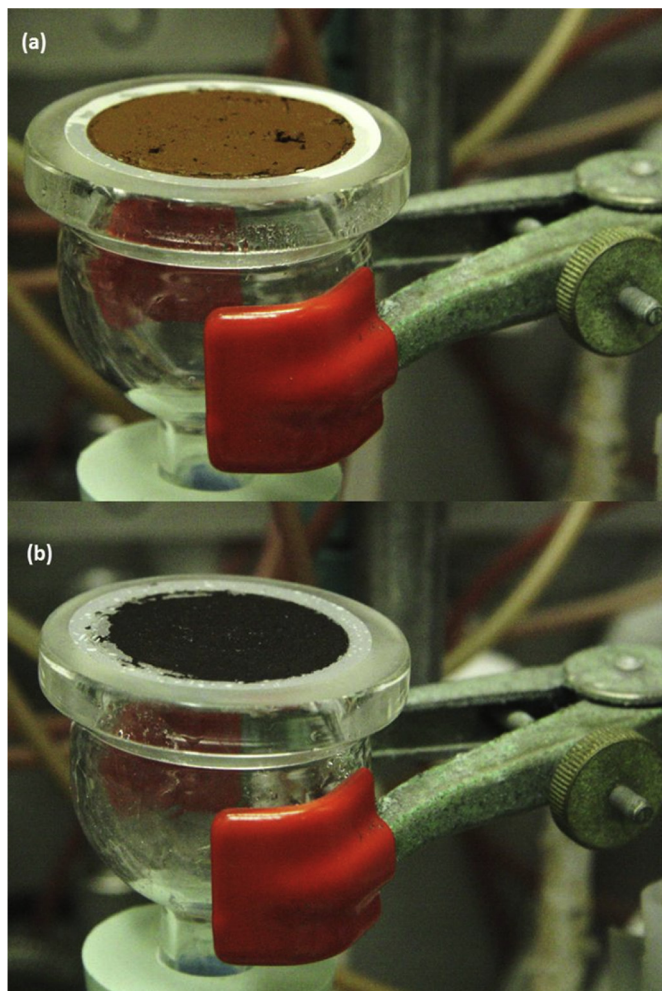
Fig. 9. Picture of uranium precipitate obtained by precipitation of U(III) in LiCl-CaCl$_2$ (30−70 mol%) at 705 °C using (a) wet argon sparging and (b) wet argon contaminated with oxygen.
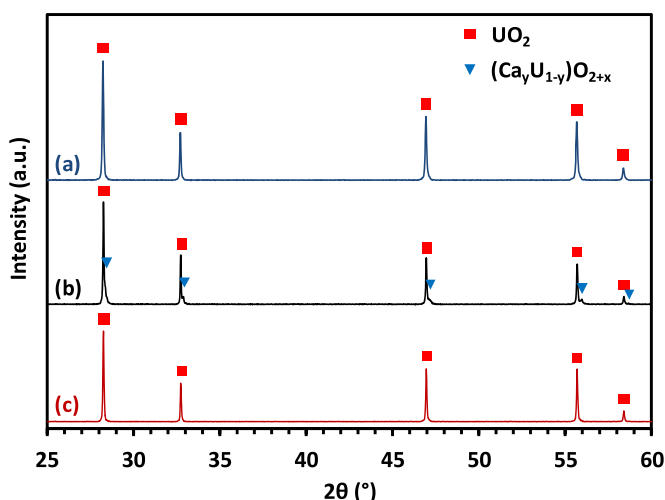

Fig. 10. XRD patterns of precipitate obtained by (a) precipitation of 5 wt% U(III) in LiCl-CaCl$_2$ (30−70 mol%) at 705 °C using wet argon sparging, (b) precipitation of 5 wt% U(III) in LiCl-CaCl$_2$ (30−70 mol%) at 705 °C using wet argon contaminated with oxygen and (c) precipitation of 5 wt% U(III) and excess of metallic uranium in LiCl-CaCl$_2$ (30−70 mol%) at 705 °C using wet argon sparging. UOCl is not observed (main diffraction peaks expected at 25.6° and 31.4°).
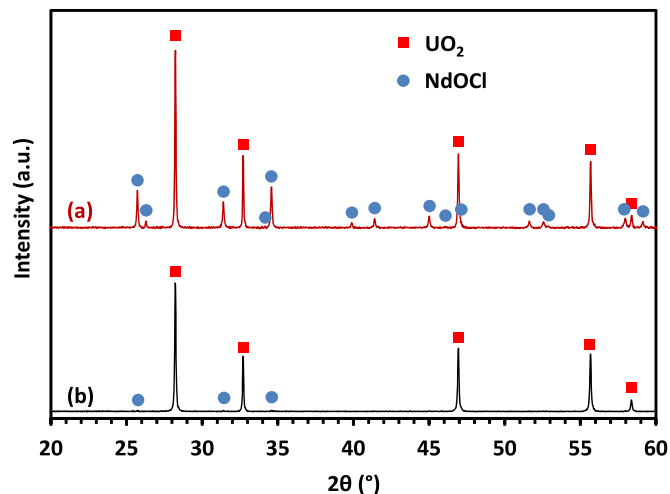

Fig. 11. XRD pattern of uranium and neodymium precipitate obtained by precipitation of 5 wt% equimolar U(III)-Nd(III) in LiCl-CaCl$_2$ (30−70 mol%) at 705 °C using wet argon sparging (a) after 6 h wet argon sparging (complete precipitation of the actinide and lanthanide of the salt) and (b) after 1 h wet argon sparging (incomplete precipitation).

4. Conclusion

The salt LiCl-CaCl$_2$ (30−70 mol%) at 705 °C used in this study for uranium(III) precipitation is oxoacid with a water dissociation constant of $10^{-4.0}$. This property leads to a low complexation of solubilized uranium, inducing its partial volatilisation during precipitation. Nevertheless, despite the use of oxoacid salt, the uranium precipitation is quantitative and there is no more solubilized uranium in the molten salt after the end of precipitation by wet argon sparging, corresponding to a conversion rate over 99.9%. U(III) precipitation leads to a red brown powder of UO$_2$ with a stoichiometric composition UO$_{2.00}$. This oxide crystallized as truncated cubes in the range of 0.2−2 μm. The amount of calcium in the precipitate is 1.2 wt% but no lithium is detected in the powder. The final oxidation state of uranium using wet argon sparging is (IV). Nevertheless, Uranium (III) is very sensitive to the oxidation, giving a second phase in the case of O$_2$ pollution of the wet argon, and inducing a strong increase of calcium contamination in the precipitate. At the opposite, the use of more reductive conditions with metallic uranium leads to a lower calcium contamination and a strong decrease the volatility of uranium by preventing UCl$_4$ formation during precipitation.

Finally, the sensitivity of uranium (III) precipitation was tested in comparison with neodymium (III) in the co-precipitation of the two elements. No solid solution was formed, due to the high precipitation reactivity of uranium leading to the consecutive precipitation of the two elements.

References

[1] H.P. Nawada, K. Fukuda, J. Phys. Chem. Solids 66 (2005) 647−651, http://dx.doi.org/10.1016/j.jpcs.2004.07.022.

[2] J. Lacquement, H. Boussier, A. Laplace, O. Conocar, A. Grandjean, J. Fluor. Chem. 130 (2009) 18—21, http://dx.doi.org/10.1016/j.jfluchem.2008.07.011.

[3] O. Conocar, N. Douyere, J. Lacquement, J. Nucl. Mater. 344 (2005) 136—141, http://dx.doi.org/10.1016/j.jnucmat.2005.04.031.

[4] E. Mendes, O. Conocar, A. Laplace, N. Douyère, M. Miguirditchian, Procedia Chem. 7 (2012) 791—797, http://dx.doi.org/10.1016/j.proche.2012.10.120.

[5] L. Martinot, M. Ligot, J. Radioanal. Nucl. Chem. Lett. 136 (1989) 53—60, http://dx.doi.org/10.1007/bf02165086.

[6] Y.H. Cho, T.-J. Kim, S.E. Bae, Y.J. Park, H.J. Ahn, K. Song, Microchem. J. 96 (2010) 344—347, http://dx.doi.org/10.1016/j.microc.2010.06.001.

[7] Y.H. Kang, S.C. Hwang, H.S. Lee, E.H. Kim, S.W. Park, J.H. Lee, J. Mater. Process. Technol. 209 (2009) 5008—5013, http://dx.doi.org/10.1016/j.jmatprotec.2009.01.024.

[8] T.-J. Kim, Y. Jung, J.-B. Shim, S.-H. Kim, S. Paek, K.-R. Kim, D.-H. Ahn, H. Lee, J. Radioanal. Nucl. Chem. 287 (2011) 347—350, http://dx.doi.org/10.1007/s10967-010-0689-z.

[9] S.H. Lee, C.H. Cho, Y.S. Lee, H.S. Lee, J.G. Kim, Korean J. Chem. Eng. 27 (2010) 1786—1790, http://dx.doi.org/10.1007/s11814-010-0410-5.

[10] T.R. Griffiths, V.A. Volkovich, J. Nucl. Mater. 274 (1999) 229—251, http://dx.doi.org/10.1016/S0022-3115(99)00091-4.

[11] A. Laplace, J.F. Vigier, T. Plet, C. Renard, F. Abraham, C. Slim, S. Delpech, G. Picard, Process for preparing an oxychloride and/or oxide of actinide(s) and/or of lanthanide(s) from a medium comprising at least one molten salt, Patent EP2760794. (2014).

[12] W.R. Grimes, J.H. Shaffer, G.M. Watson, Preparation of refractory oxide crystals, Patent US3063795. (1962).

[13] J.F. Vigier, C. Renard, A. Laplace, J. Lacquement, F. Abraham, J. Nucl. Mater. 432 (2013) 407—413, http://dx.doi.org/10.1016/j.jnucmat.2012.08.039.

[14] J.-F. Vigier, C. Renard, N. Henry, A. Laplace, F. Abraham, Inorg. Chem. 51 (2012) 4352—4358, http://dx.doi.org/10.1021/ic3000558.

[15] K.H. Mahendran, S. Nagaraj, R. Sridharan, T. Gnanasekaran, J. Alloys Compd. 325 (2001) 78—83, http://dx.doi.org/10.1016/S0925-8388(01)01387-1.

[16] D.R. Lide, Handbook of Chemistry and Physics 73rd Edition, 1992-1993.

[17] I. Grenthe, J. Drożdżyński, T. Fujino, E.C. Buck, T.E. Albrecht-Schmitt, S.F. Wolf, in: L.R. Morss, N.M. Edelstein, J. Fuger (Eds.), Uranium The Chemistry of the Actinide and Transactinide Elements, Springer Netherlands, 2006, pp. 253—698, http://dx.doi.org/10.1007/978-94-007-0211-0_5.

[18] J. Drozdzynski, Coord. Chem. Rev. 249 (2005) 2351—2373, http://dx.doi.org/10.1016/j.ccr.2005.05.016.

[19] C. Caravaca, A. Laplace, J. Vermeulen, J. Lacquement, J. Nucl. Mater. 377 (2008) 340—347, http://dx.doi.org/10.1016/j.jnucmat.2008.01.031.

[20] Y. Castrillejo, M.R. Bermejo, E. Barrado, A.M. MartInez, P. Diaz Arocas, J. Electroanal. Chem. 545 (2003) 141—157, http://dx.doi.org/10.1016/s0022-0728(03)00092-5.

[21] F.C. Zeisberg, International Critical Tables, Partial Vapor Pressures of Aqueous Solutions of HCl, Vol. III, Vapor Pressure Lowering, 1928, p. 292.

[22] V. Petříček, M. Dušek, L. Palatinus, Z. Krist. 229 (2014) 345, http://dx.doi.org/10.1515/zkri-2014-1737.

[23] V.L. Cherginets, E.G. Khailova, Electrochim. Acta 39 (1994) 823—829, http://dx.doi.org/10.1016/0013-4686(94)80031-6.

[24] B. Trémillon, Electrochimie analytique et réaction en solution, Tome 1 (1993).

[25] E. Mendes, O. Conocar, A. Laplace, N. Douyère, J. Lacquement, M. Miguirditchian, Actinides oxidative back-extraction from liquid aluminium, in molten chloride media, in: Molten Salts Chemistry and Technology, John Wiley & Sons, Ltd, 2014, pp. 411—419, http://dx.doi.org/10.1002/9781118448847.ch6c.

[26] R. Combes, B. Tremillon, F. Deandrade, M. Lopes, H. Ferreira, Anal. Lett. 15 (1982) 1585—1600, http://dx.doi.org/10.1080/00032718208064449.

[27] D.M. Gruen, R.L. McBeth, J. Inorg. Nucl. Chem. 9 (1959) 290—301, http://dx.doi.org/10.1016/0022-1902(59)80233-5.

[28] V.A. Volkovich, D.E. Aleksandrov, B.D. Vasin, T.K. Khabibullin, D.S. Mal'tsev, Rasplavy, 2009, pp. 62—68.

[29] G. Leinders, T. Cardinaels, K. Binnemans, M. Verwerft, J. Nucl. Mater. 459 (2015) 135—142, http://dx.doi.org/10.1016/j.jnucmat.2015.01.029.

[30] L. Mazeina, A. Navrotsky, M. Greenblatt, J. Nucl. Mater. 373 (2008) 39—43, http://dx.doi.org/10.1016/j.jnucmat.2007.03.269.

[31] A. Pialoux, B. Touzelin, J. Nucl. Mater. 255 (1998) 14—25, http://dx.doi.org/10.1016/s0022-3115(98)00015-4.

[32] T. Ohmichi, S. Fukushima, A. Maeda, H. Watanabe, J. Nucl. Mater. 102 (1981) 40—46, http://dx.doi.org/10.1016/0022-3115(81)90544-4.

[33] G. Meyer, T. Schleid, Z. Anorg. Allg. Chem. 533 (1986) 181—185, http://dx.doi.org/10.1002/zaac.19865330222.